



Turbulent bubbly flow under breaking water waves

Jim Kirby and Morteza Derakhti

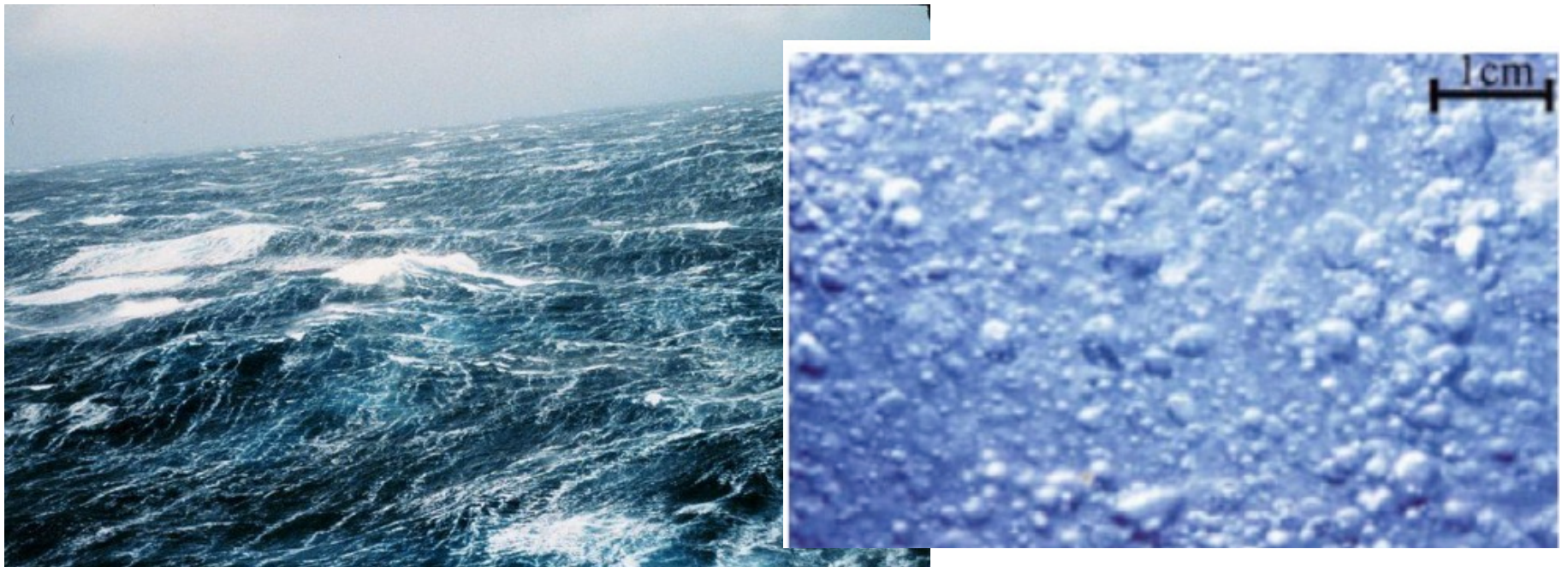
CACR, Dept. of Civil and Environmental Engineering, University of Delaware

USNCCM13, San Diego, July 27, 2015

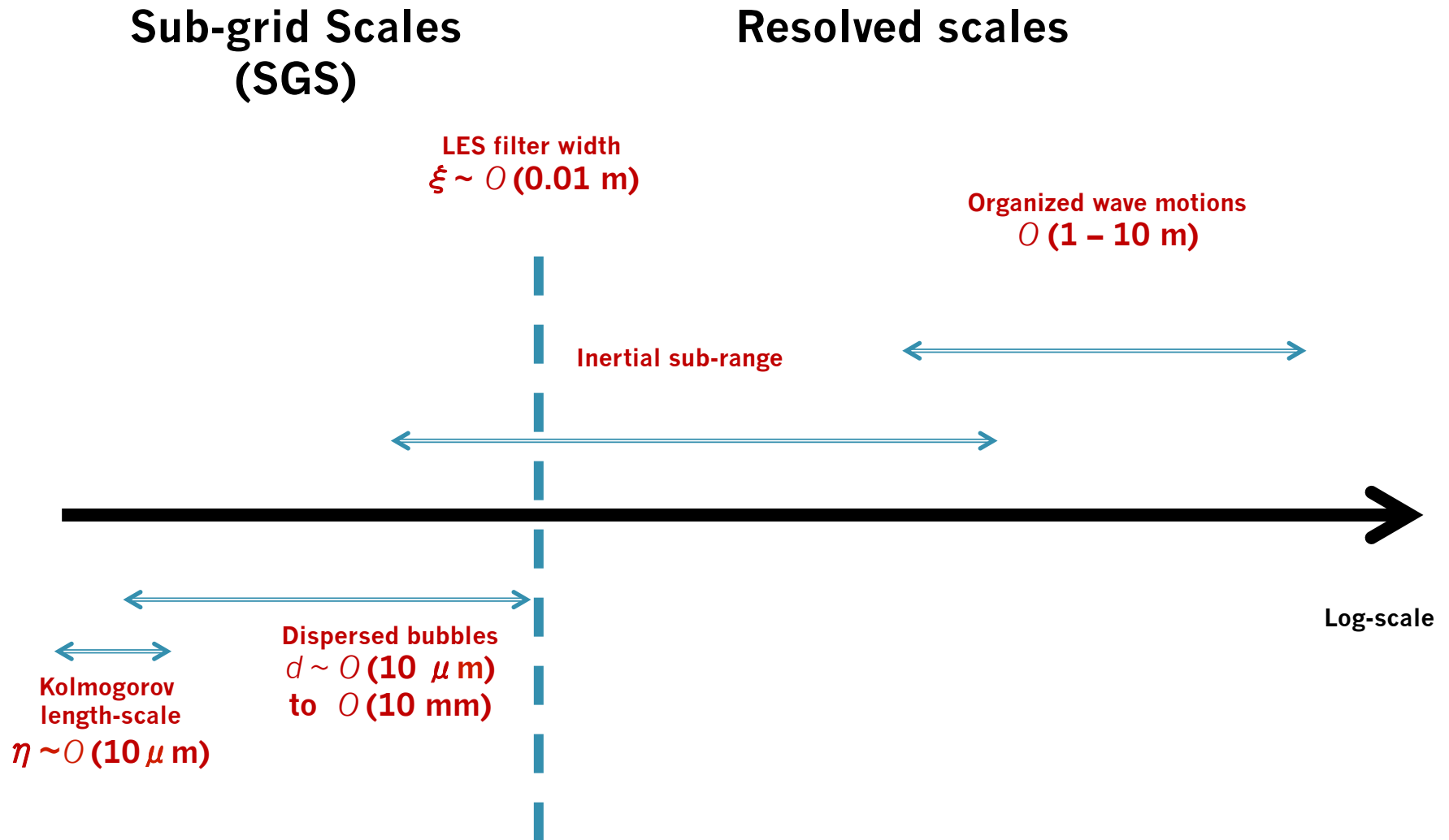


Motivation

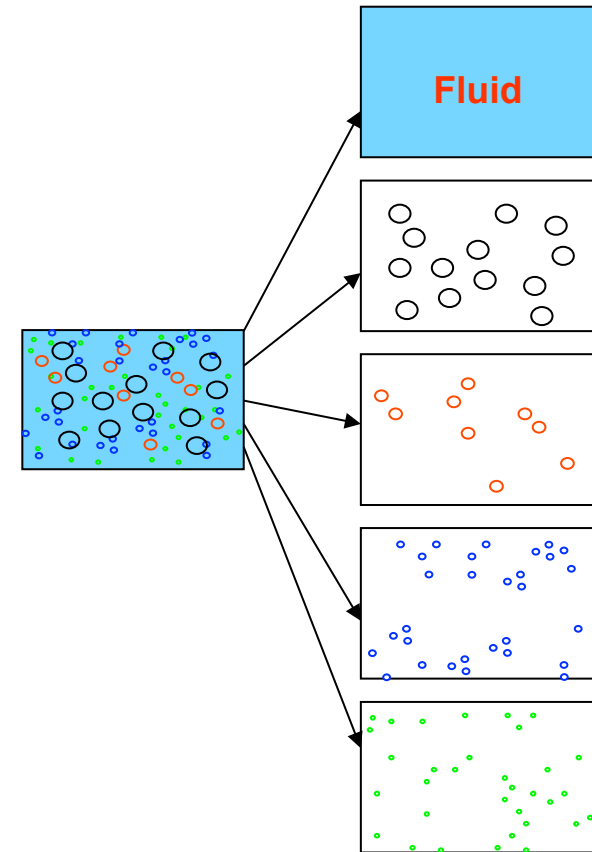
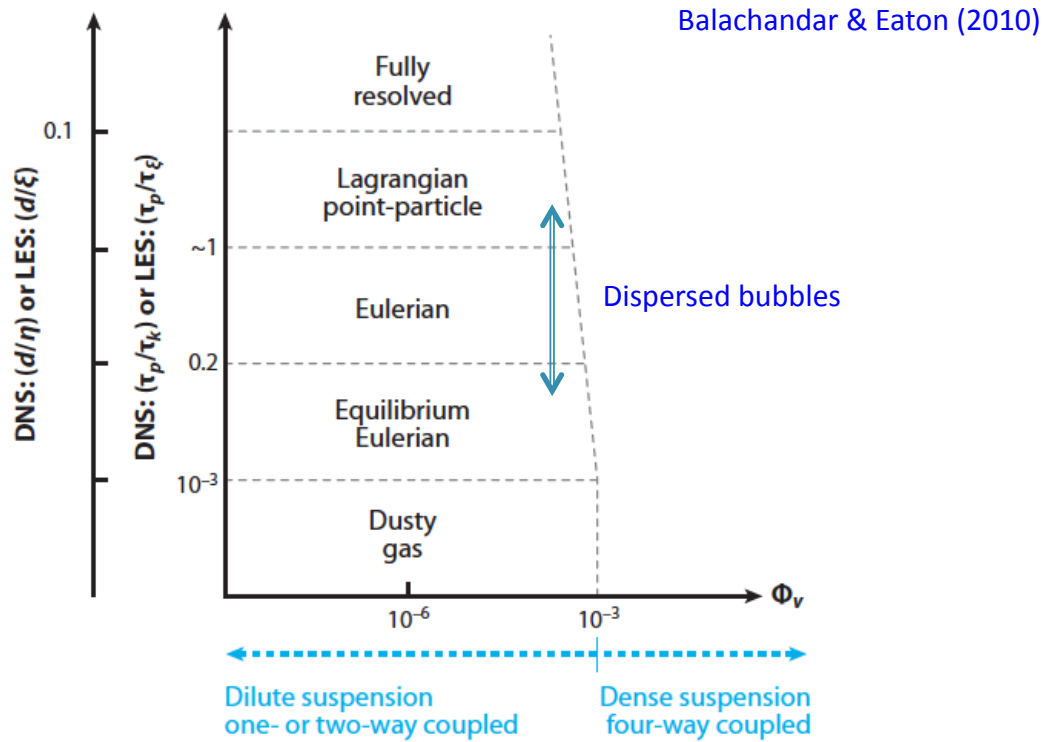
- Underwater optical and acoustical properties, atmosphere/ocean gas transfer
- Turbulence modulation by bubbles under breaking waves
- Link between dissipation and mixing processes



Why LES? Range of spatial scales



Turbulent multiphase flow



d_b (mm)	w_b (m/s)	$St(\varepsilon = 0.01)$	$St(\varepsilon = 0.1)$	$St(\varepsilon = 1.0)$
1	0.15	0.014	0.031	0.066
3	0.23	0.051	0.110	0.236
5	0.23	0.102	0.219	0.472
8	0.23	0.191	0.412	0.887
10	0.23	0.258	0.555	1.196

Table 1.1: Bubble Stokes number for different bubble diameters and turbulence dissipation rates. w_b is the rise velocity of a bubble.

Filtered poly-disperse two-fluid model

(Carrica et al. 1999, Ma et al. 2011, Lakehal et al. 2002, Derakhti&Kirby 2014)

- Liquid phase**

$$\frac{\partial(\alpha^l \rho^l)}{\partial t} + \frac{\partial}{\partial x_j}(\alpha^l \rho^l \tilde{u}_j^l) = 0$$

$$\frac{\partial(\alpha^l \rho^l \tilde{u}_i^l)}{\partial t} + \frac{\partial}{\partial x_j}(\alpha^l \rho^l \tilde{u}_i^l \tilde{u}_j^l) = -\frac{\partial}{\partial x_j}(\alpha^l \tilde{p}) \delta_{ij} + \alpha^l \rho^l g_i + \frac{\partial}{\partial x_j} [\alpha^l (\tilde{\sigma}_{ij}^l - \tau_{ij}^l)] + M^{gl}$$

- Gas phase**

$$\frac{\partial N_k^g}{\partial t} + \frac{\partial}{\partial x_j}(\tilde{u}_{k,j}^g N_k^g) = B_k^g + S_k^g$$

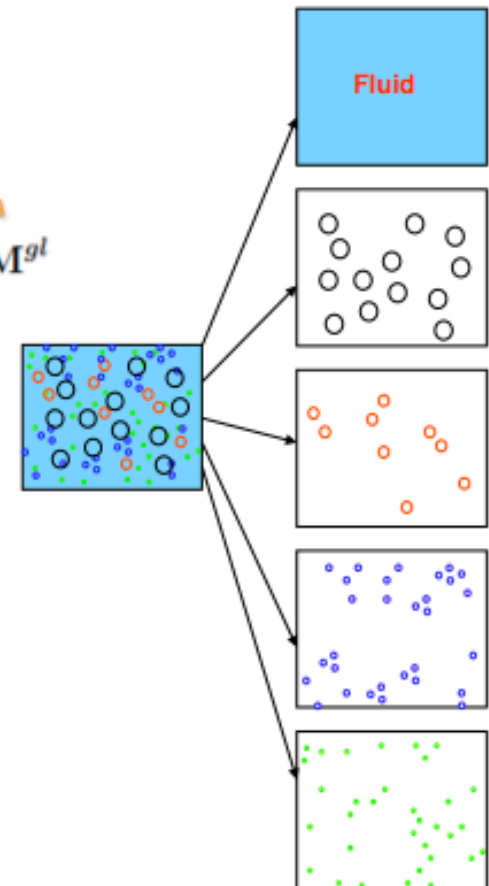
$$0 = -\frac{\partial}{\partial x_j}(\alpha_k^g \tilde{p}) \delta_{ij} + \alpha_k^g \rho^g g_i + M_k^{lg} \quad k = 1, \dots, NG$$

Drag, lift and added mass forces

Bubble entrainment

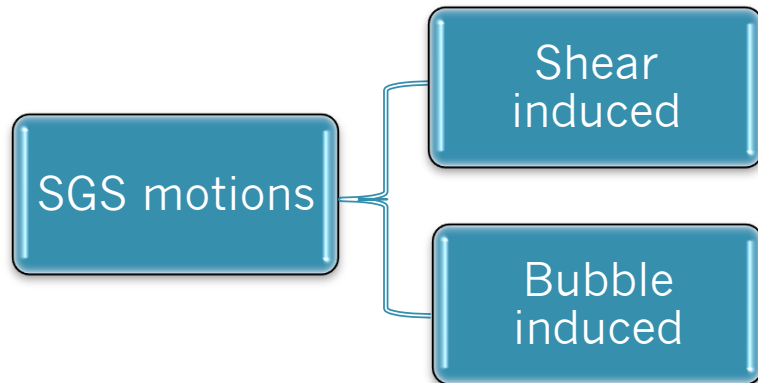
Bubble break up

NG is the number of bubble classes



Numerical implementation in TRUCHAS
(Rider and Kothe, 1998)

Closure models for poly-disperse LES



- Eddy viscosity approach:

$$\tilde{\sigma}_{ij}^l - \tau_{ij}^{l,d} = 2\nu_{eff}^l \tilde{S}_{ij}$$

$$\nu_{eff}^l = \nu^l + \nu_{sgs}^l + \nu_{BI}^l$$

$$\nu_{sgs}^l = (C_s \Delta)^2 |\tilde{S}|$$

$$\nu_{BI}^l = C_{BIT} \sum_{i=1}^{NG} \alpha_k^g d_k |\tilde{u}_j^l - \tilde{u}_{k,j}^l|$$

Sato and Sekogushi

- Dynamic Smagorinsky model (DSM)**

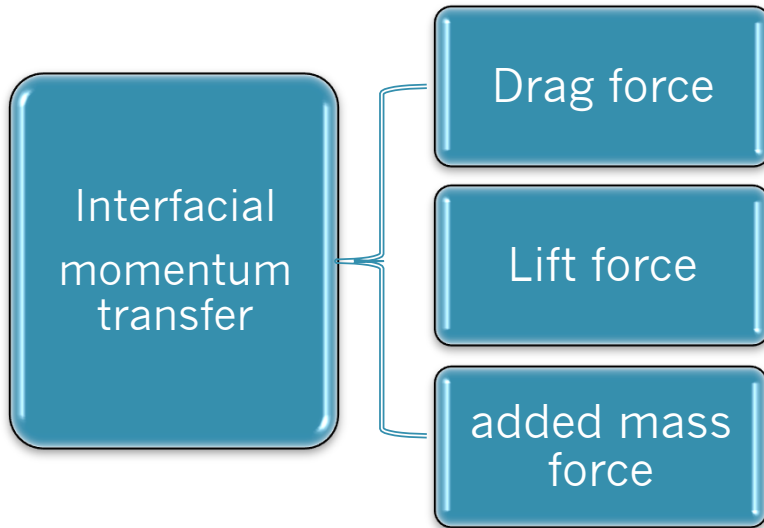
- C_s^2 computed dynamically using the double filtered flow velocities proposed by Germano et al. (1991) and Lilly (1992)
- Converges to zero turbulent viscosity when flow is not turbulent
- The only input parameter is the filter width ratio
- Need averaging, here we follow the Zang et al (1993) and use the local averaging
- We used the box filter for the test filter

$$(C_s)^2 = -\frac{L_{ij} M_{ij}}{2\tilde{\Delta}^2 M_{ij} M_{ij}}$$

$$L_{ij} = \widehat{\tilde{u}_i^l \tilde{u}_j^l} - \widehat{\tilde{u}_i^l} \widehat{\tilde{u}_j^l}, \quad M_{ij} = \alpha^2 |\widehat{\tilde{S}}| \widehat{\tilde{S}}_{ij} - \widehat{|\tilde{S}| \tilde{S}_{ij}}$$

$\widehat{\quad}$ represent the test scale filter
with $\widehat{\Delta}$ width greater than the $\tilde{\Delta}$ and $\alpha = \widehat{\Delta}/\tilde{\Delta} > 1$.

Closure models for poly-disperse LES



Bubble entrainment

$$\mathbf{M}_k^{lg} = \tilde{\mathbf{f}}_k^{VM} + \tilde{\mathbf{f}}_k^L + \tilde{\mathbf{f}}_k^D,$$

$$\tilde{\mathbf{f}}_k^{VM} \approx \alpha_k^b \rho^l C_{VM} \left(\frac{D\tilde{\mathbf{u}}^l}{Dt} - \frac{D\tilde{\mathbf{u}}_k^b}{Dt} \right)$$

$$\tilde{\mathbf{f}}_k^L \approx \alpha_k^b \rho^l C_L (\tilde{\mathbf{u}}^l - \tilde{\mathbf{u}}_k^b) \times (\nabla \times \tilde{\mathbf{u}}^l)$$

$$\tilde{\mathbf{f}}_k^D \approx \alpha_k^b \rho^l \frac{3}{4} \frac{C_D}{d_k^b} (\tilde{\mathbf{u}}^l - \tilde{\mathbf{u}}_k^b) |\tilde{\mathbf{u}}^l - \tilde{\mathbf{u}}_k^b|,$$

- We connect the volume of the entrained bubbles to the local liquid turbulence near the free surface:

$$B_k^g = \frac{c_b}{4\pi} \left(\frac{\sigma}{\rho^l} \right)^{-1} \alpha^l \frac{f(a_k) \Delta a_k}{\sum_{k=1}^{NG} a_k^2 f(a_k) \Delta a_k} \mathcal{P}_{sgs}^l,$$

$$\mathcal{P}_{sgs}^l = 2\nu_{sgs}^l \tilde{S}_{ij} \tilde{S}_{ij} = \nu_{sgs}^l |\tilde{S}|^2.$$

- Initial size distribution (**Deane&Stokes**):

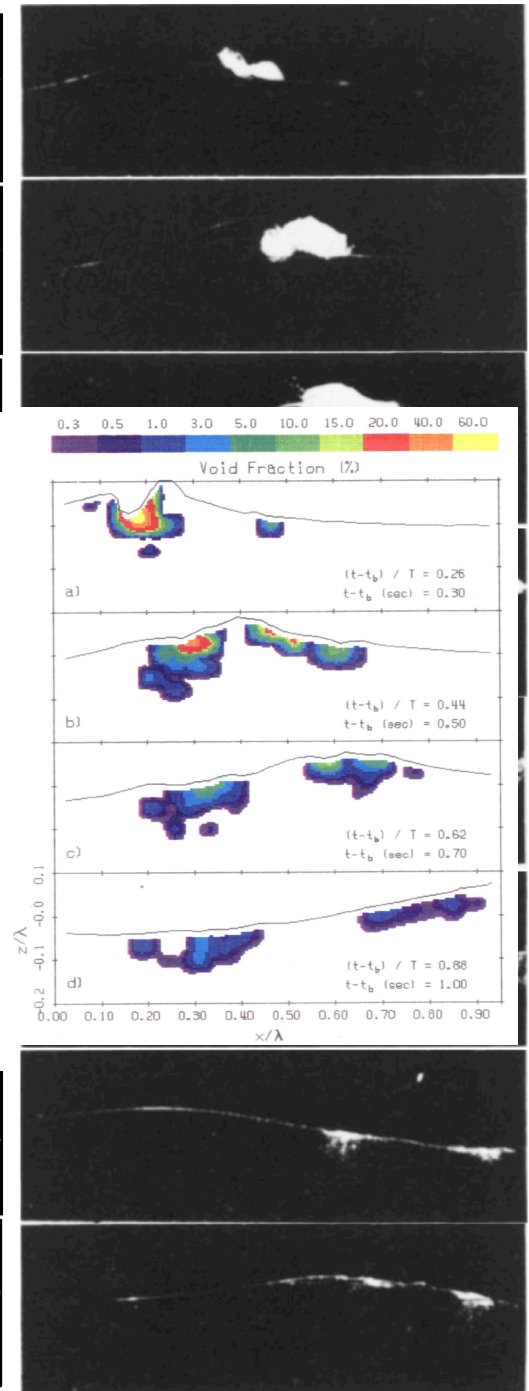
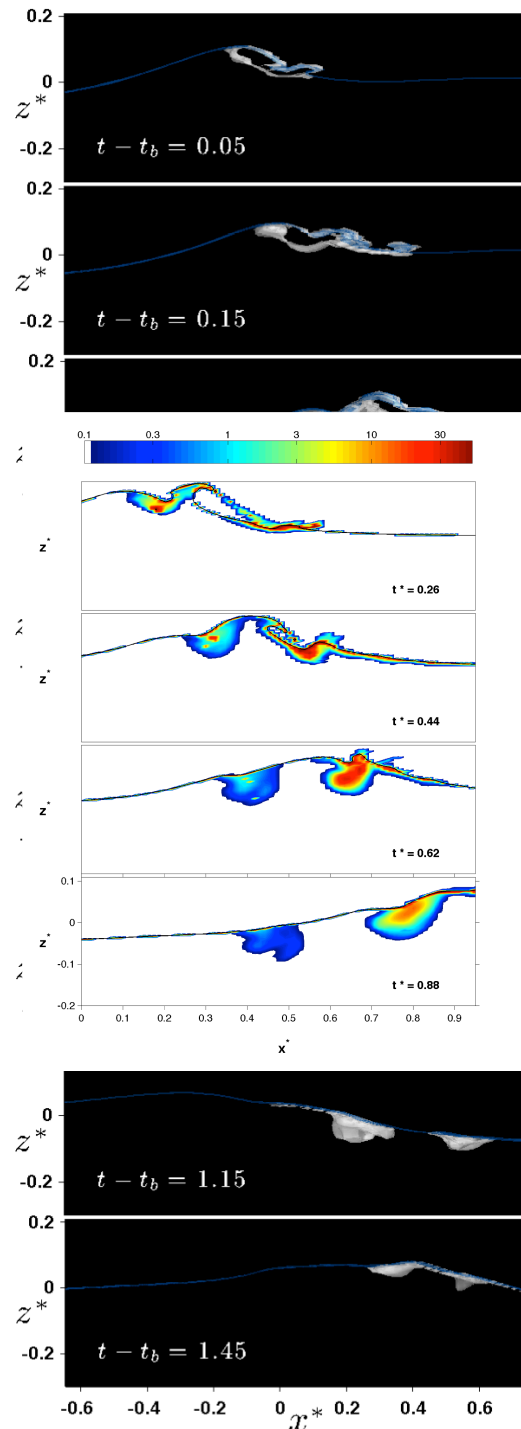
$$\begin{aligned} f(a) &\propto a^{-10/3} & \text{if } a \geq 1.0\text{mm} \\ f(a) &\propto a^{-3/2} & \text{if } a \leq 1.0\text{mm} \end{aligned}$$

Model validation

- Extensive model validation has been done for steepness-limited breaking waves generated by dispersive focusing (Derakhti & Kirby, JFM 2014):

- Short waves, followed by faster long waves, focus at a predefined location
- Snapshots of free surface evolution
- Evolution of bubble void fraction comparing to the photographs taken by Rapp and Melville (1990)

- Evolution of bubble void fraction comparing to the measurements by Lamarre and Melville (1991): Large plunging breaker



Total dissipation per unit length of breaking crest

- Bubble-induced dissipation accounts for more than 50% of the total dissipation, which is compatible with the measurements of potential energy of the bubble plume by Lamarre and Melville (1991).
- Although the total dissipation differs between different breaker types, the ratio of bubble- and shear-induced dissipation is invariant with respect to breaking type and intensity.
- The corresponding simulations without the inclusion of dispersed bubbles underpredict the total dissipation by about 35%.

Case no.	LM (J/m)	$\hat{\epsilon}_{total}(J/m)$	$\hat{\epsilon}_{total}^{nb}/\hat{\epsilon}_{total}$ (%)	$\hat{\epsilon}_{sgs}^{SI}/\hat{\epsilon}_{total}$ (%)	$\hat{\epsilon}_{sgs}^{BI}/\hat{\epsilon}_{total}$ (%)
Large plunging	17.8	14.7	63.7	45.9	52.9
Plunging	8.6	7.7	64.8	45.4	53.0
Weakly plunging/spilling	4.3	2.6	65.9	43.2	53.7
Spilling		1.4	64.5	42.3	51.6

Integrated TKE

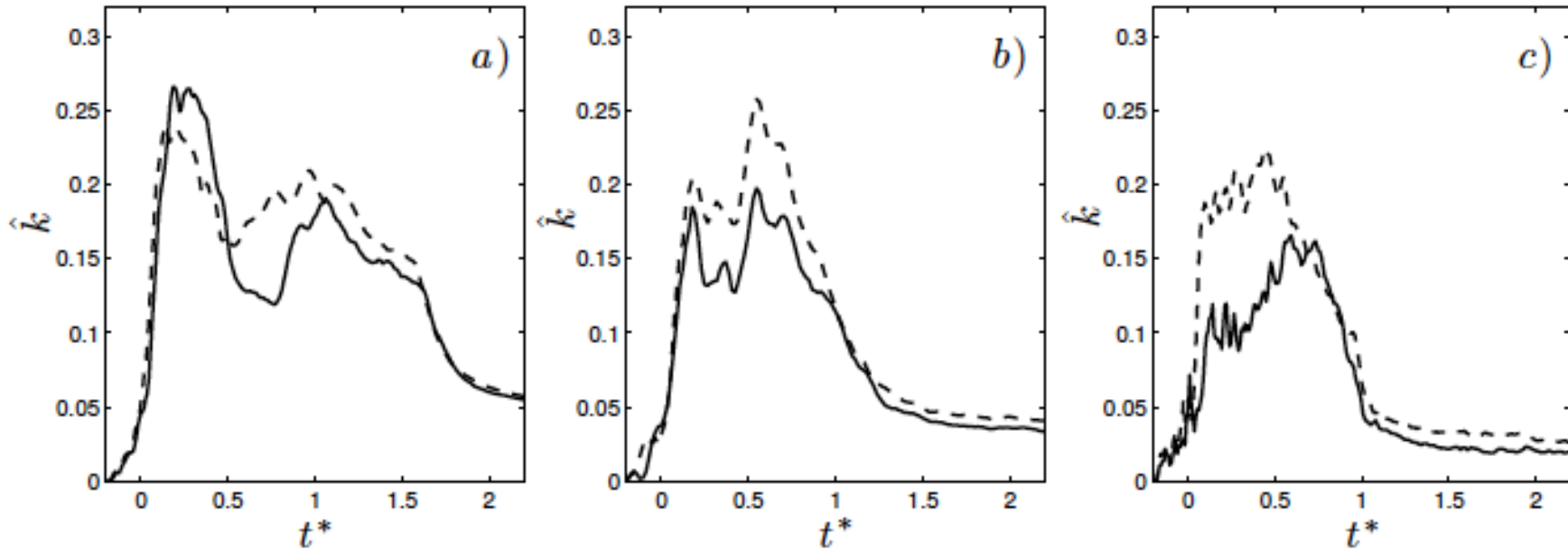


FIGURE 28. Normalized total resolved TKE, \hat{k} , in the breaking region, — simulation with dispersed bubbles and - - - simulation without inclusion of the dispersed bubbles for (a) P1; (b) SP1 and (c) S1. The reference value is $L_c^2 C_c^2 (S - S_0) S_0^4$. The results have been smoothed using two adjacent points.

- integrated TKE in the breaking region is damped by the dispersed bubbles about 20% for the large plunging breaker to 50% for the spilling breakers.
- In the plunging breakers, TKE is damped slightly or even enhanced during the initial stage of active breaking.

Moving to the surfzone

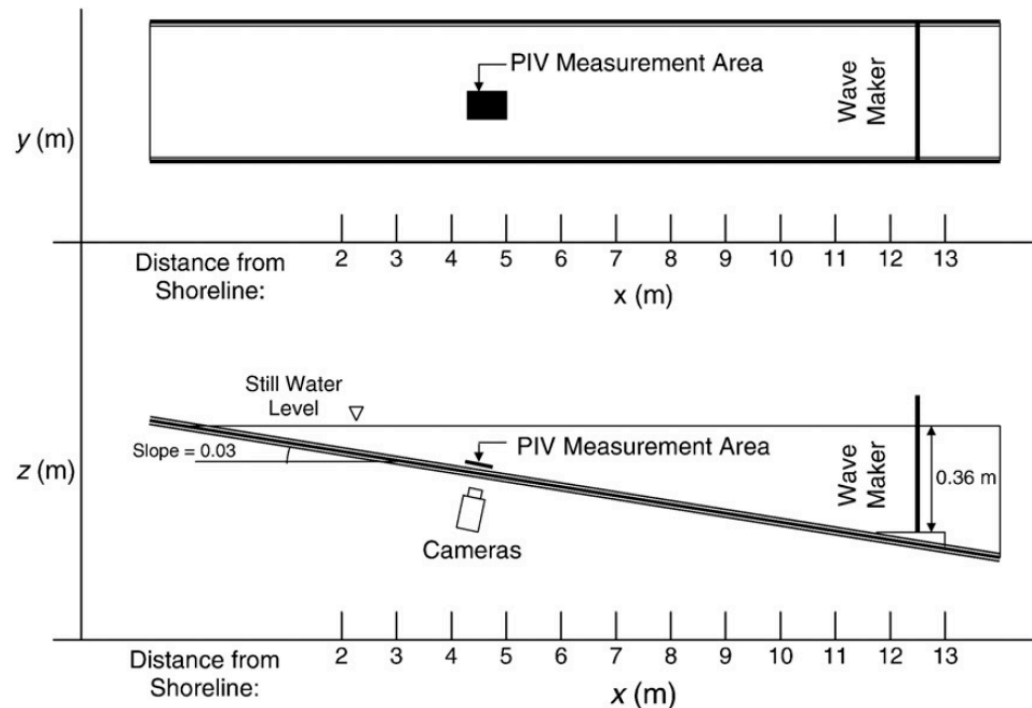
- 1) What are the physical characteristics of coherent structures (CS) generated by breaking waves in the surf zone?
- 2) What role do the CS play in determining the vertical distribution of air in the water column?

Periodic surf zone breaking waves

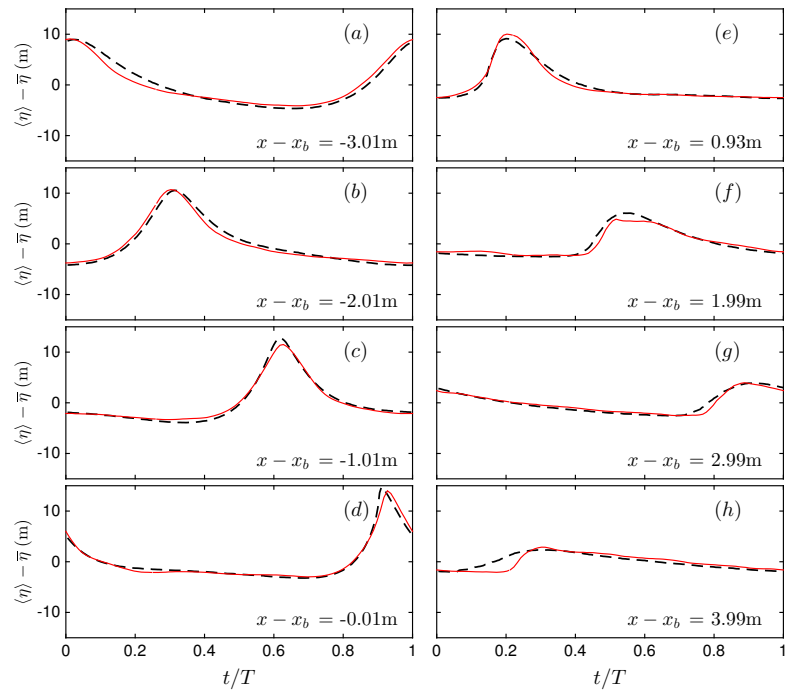
Ting & Nelson (2011)

Ting et al (2013)

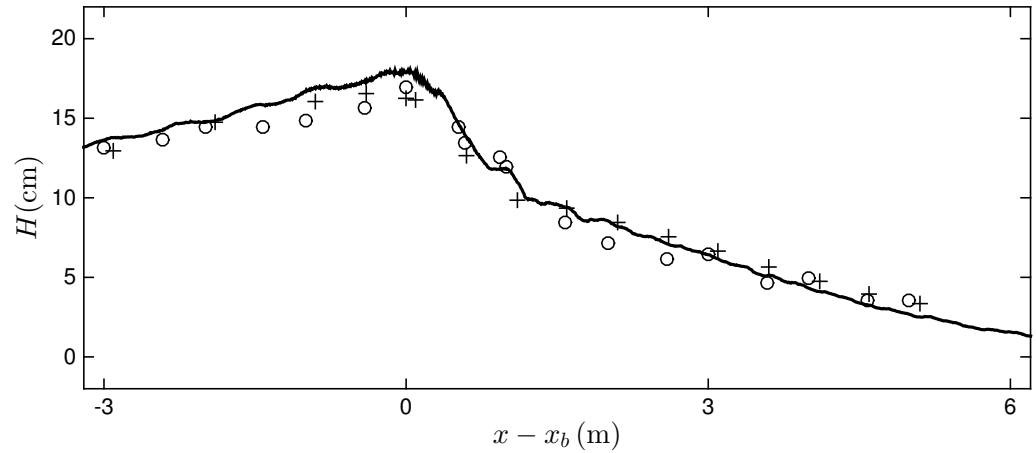
- Cnoidal waves with $H = 0.122$ m and $T = 2$ s
- Weakly plunging/spilling breaker
- $\Delta x = 25$ mm, $\Delta y = \Delta z = 7$ mm



Periodic spilling breakers: wave profiles and wave height



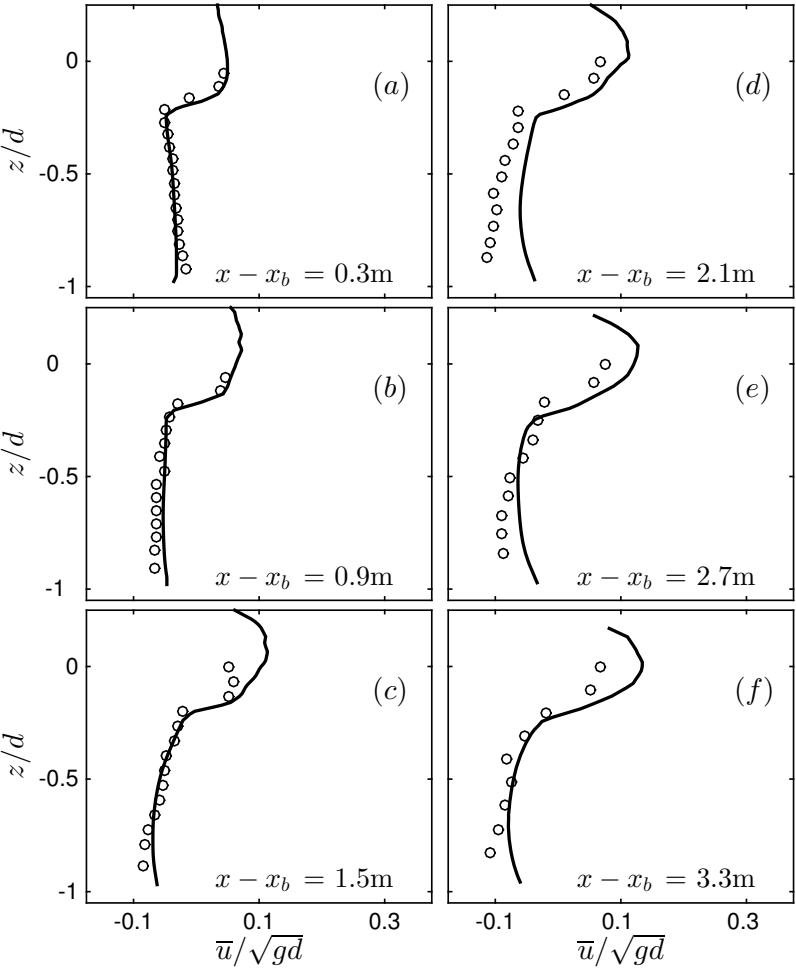
Wave profiles in surfzone



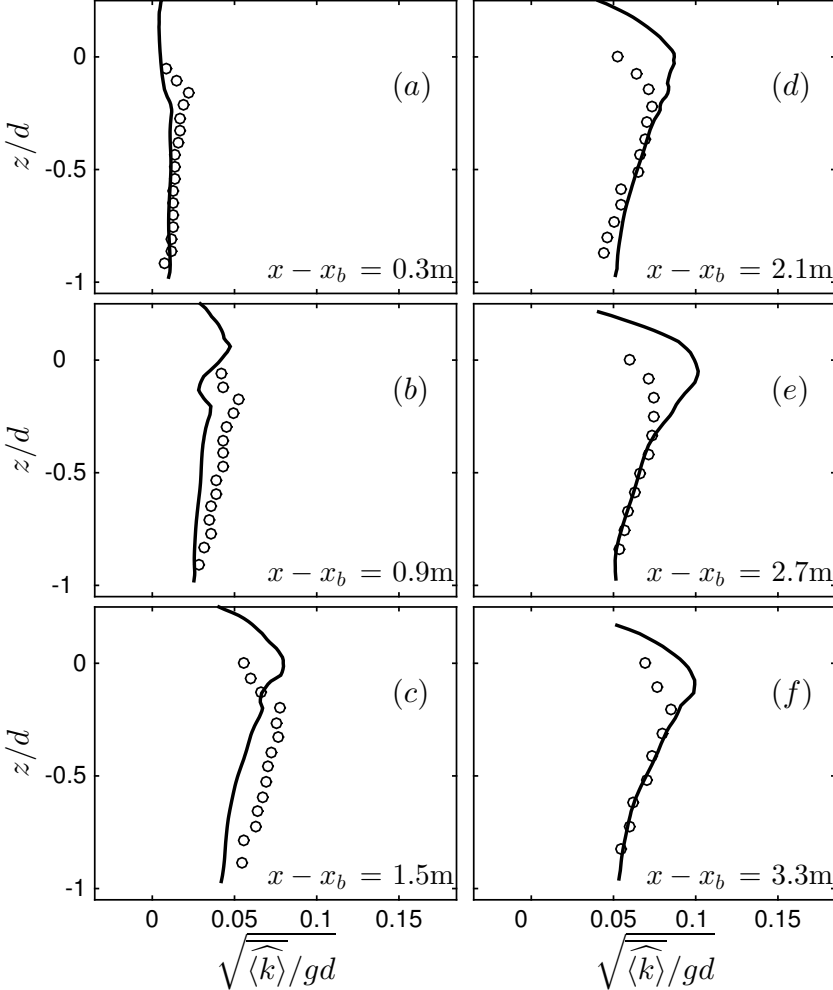
Wave height across surfzone.

Data: Ting and Nelson (2011) o
 Ting and Kirby (1996) +

Periodic spilling breakers: profiles of mean u , k



undertow



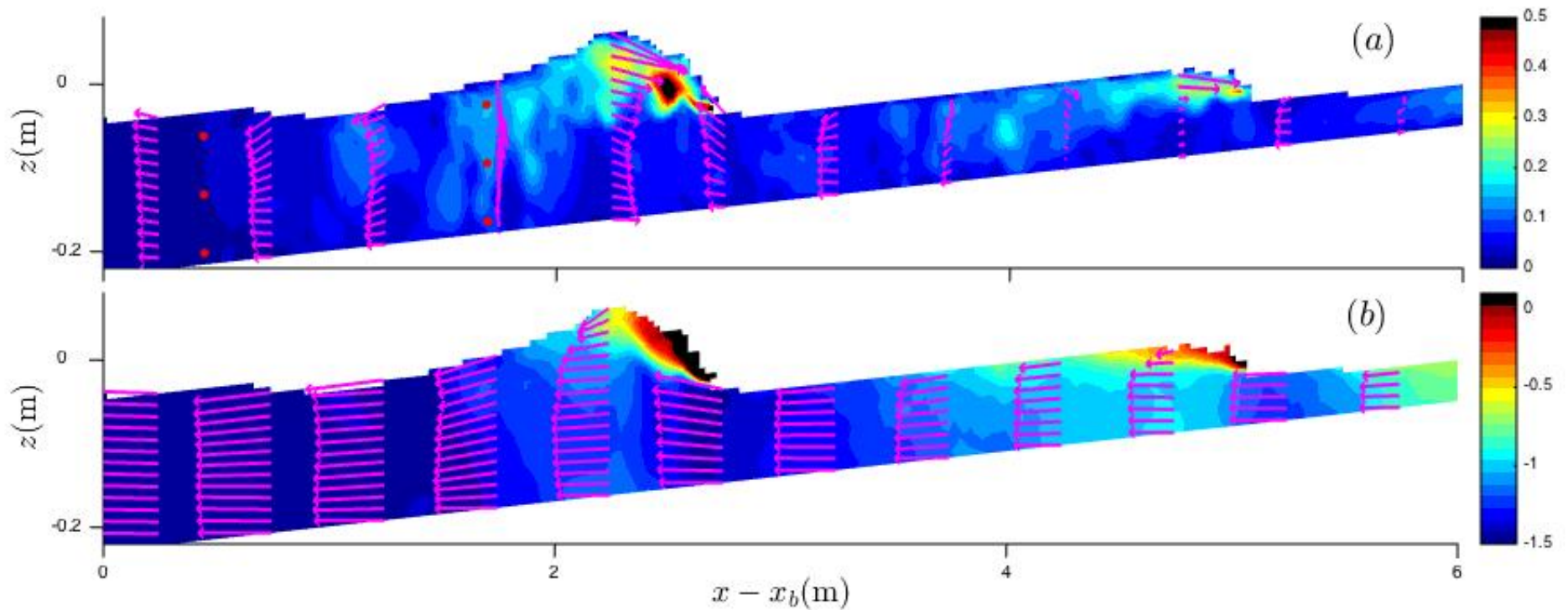
TKE

Phase – and spanwise-averaged velocities.

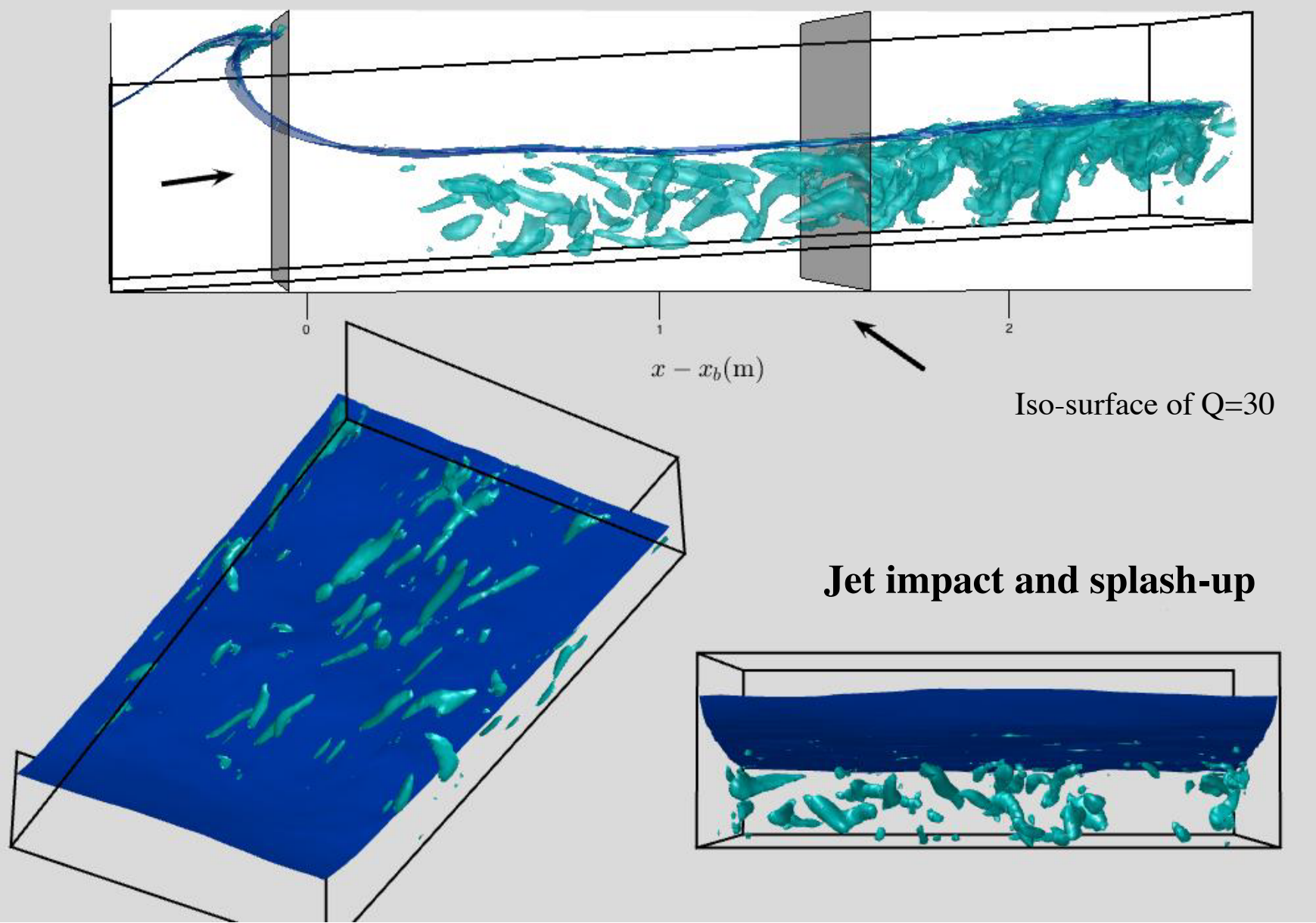
Color scale is for u'_{rms} .

Top: velocities in stationary coordinates

Bottom: velocities in wave-following frame $(u-(gh)^{1/2})$



Vortex structures (VS) identified by Q criterion



CS in lab: PIV measurements

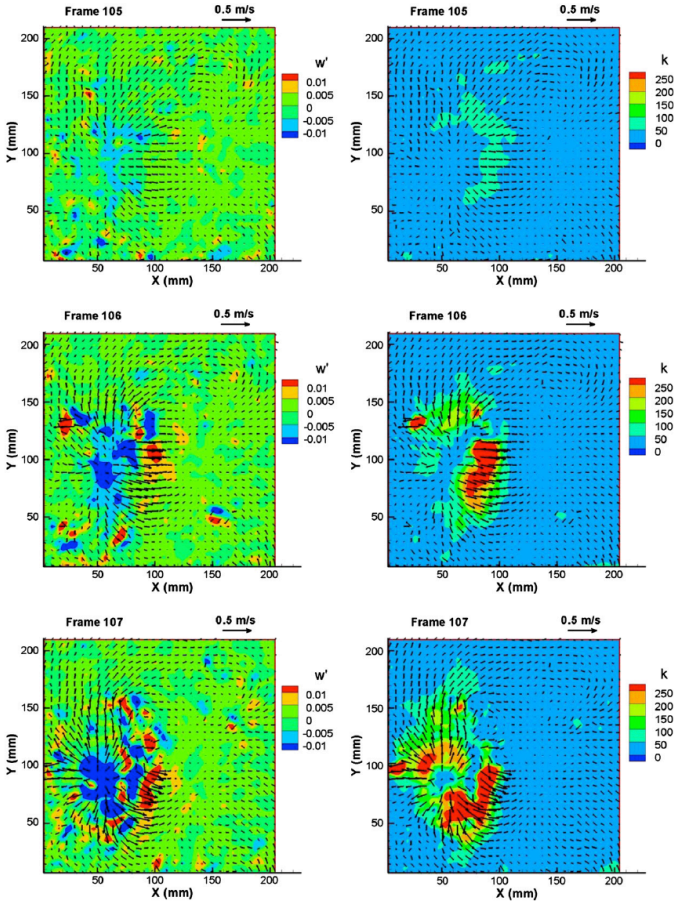


Fig. 15. Instantaneous turbulent velocity fields from Test 9, left FOV, 4th wave cycle. The contour variables are w' in m/s (left column) and $k = (u'^2 + v'^2 + w'^2)/2$ in cm^2/s^2 (right column). The breaking waves propagate in the $-X$ direction. The wave crest passes in frame 101; flow reversal occurs in frame 106; and the wave trough passes in frame 123 (15 frames = 1 s).

Ting and Nelson (2011)

Ting et al (2013)

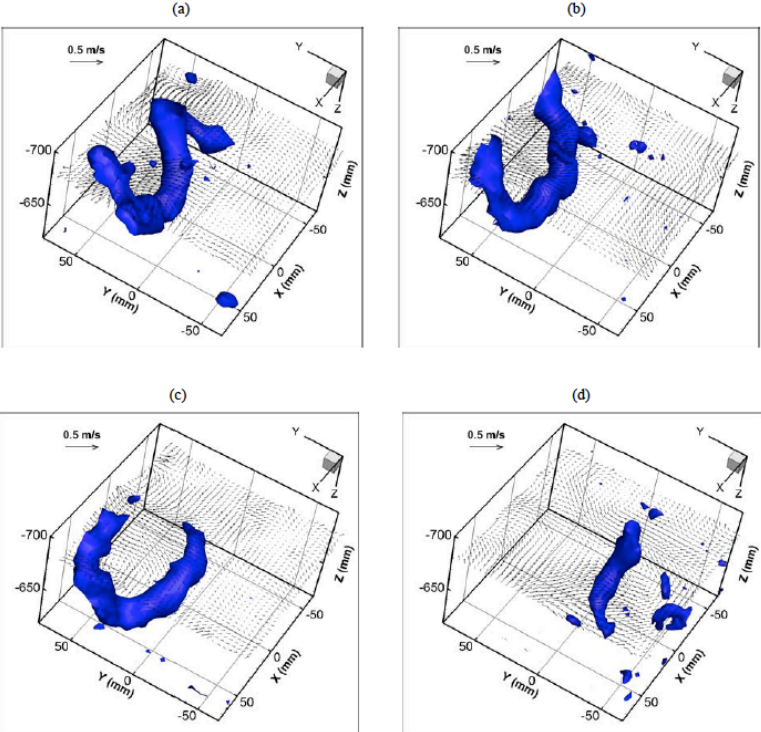


Figure 9: Measured velocity fields and iso-surfaces of $\lambda_2 = -60$ showing a vortex loop depending to the bottom after

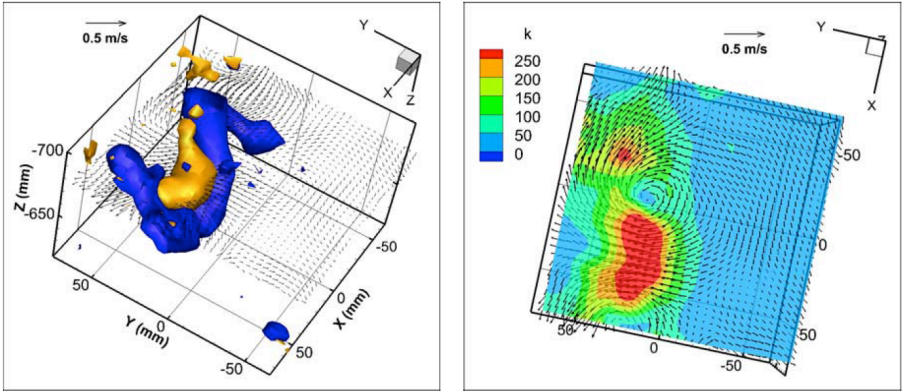
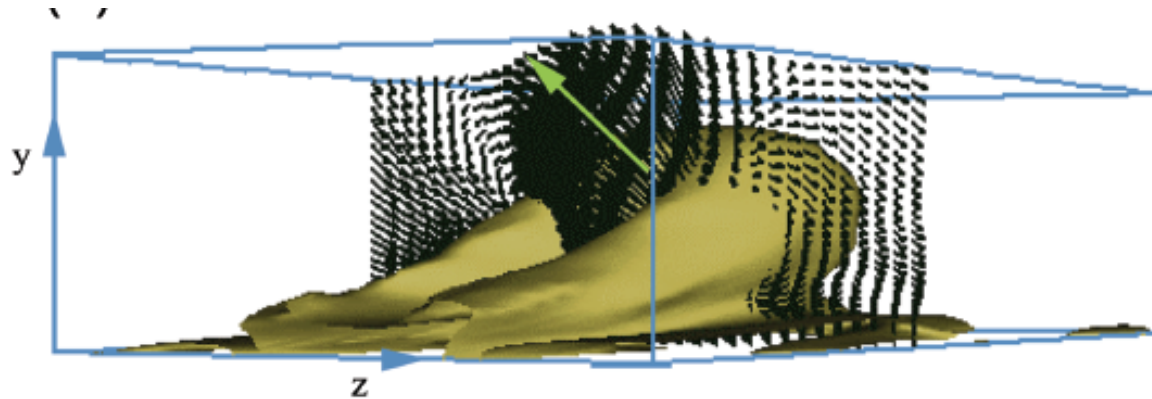


Figure 11: (Left) Iso-surfaces of $\lambda_2 = -60$ (dark blue color) and $k = 250 \text{ cm}^2/\text{s}^2$ (orange color). (Right) Turbulent kinetic energy in X - Y plane at $Z = -676 \text{ mm}$; the contour variable is $k = (U^2 + V^2 + W^2)/2$ in cm^2/s^2 . The bottom of the flume is located at $Z = -611 \text{ mm}$.

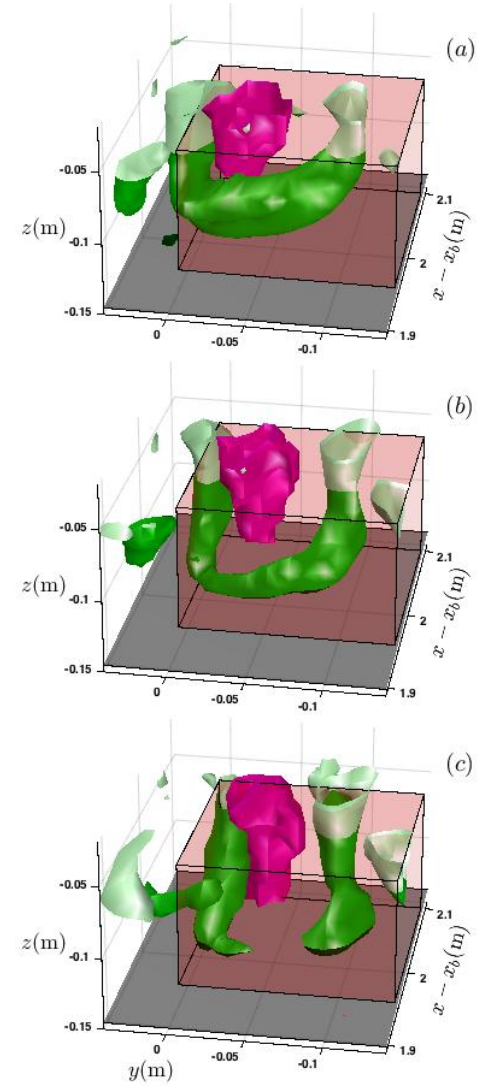
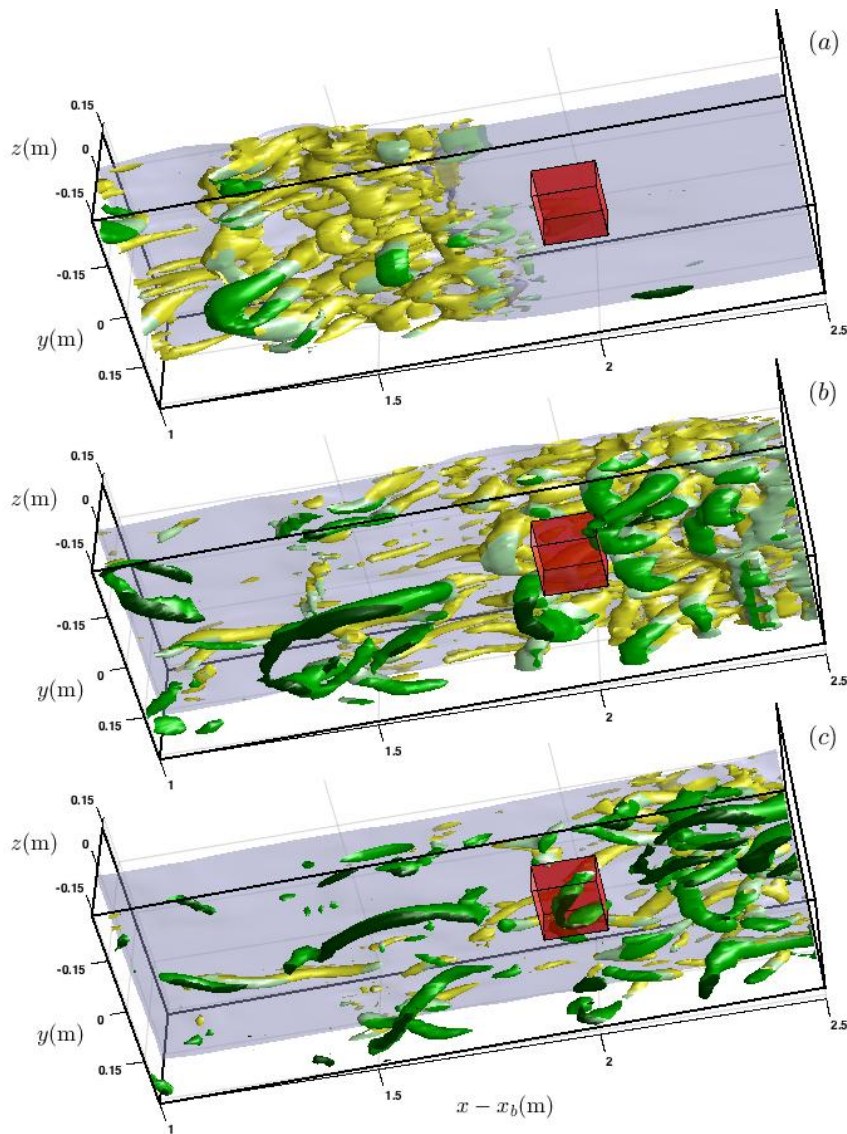
Classification of coherent structures

- Vortex structures (VS): $Q > 30$
 - “Downbursts” (DBS): $w' < 0$, Reynolds stress $> 2 u'_{\text{rms}} w'_{\text{rms}}$
 - “Upbursts” (UBS): $w' > 0$, Reynolds stress $> 2 u'_{\text{rms}} w'_{\text{rms}}$
- (both “burst” cases require $Q < 30$)

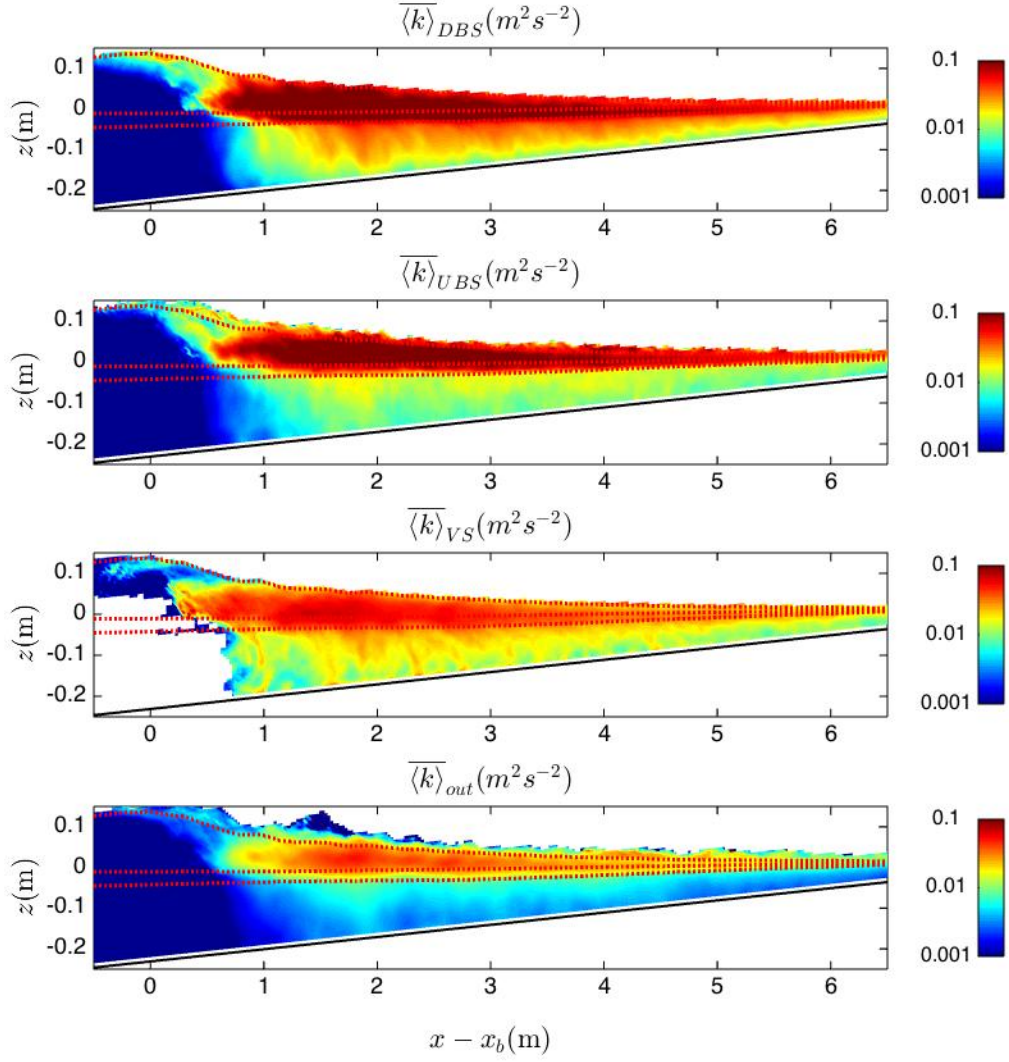
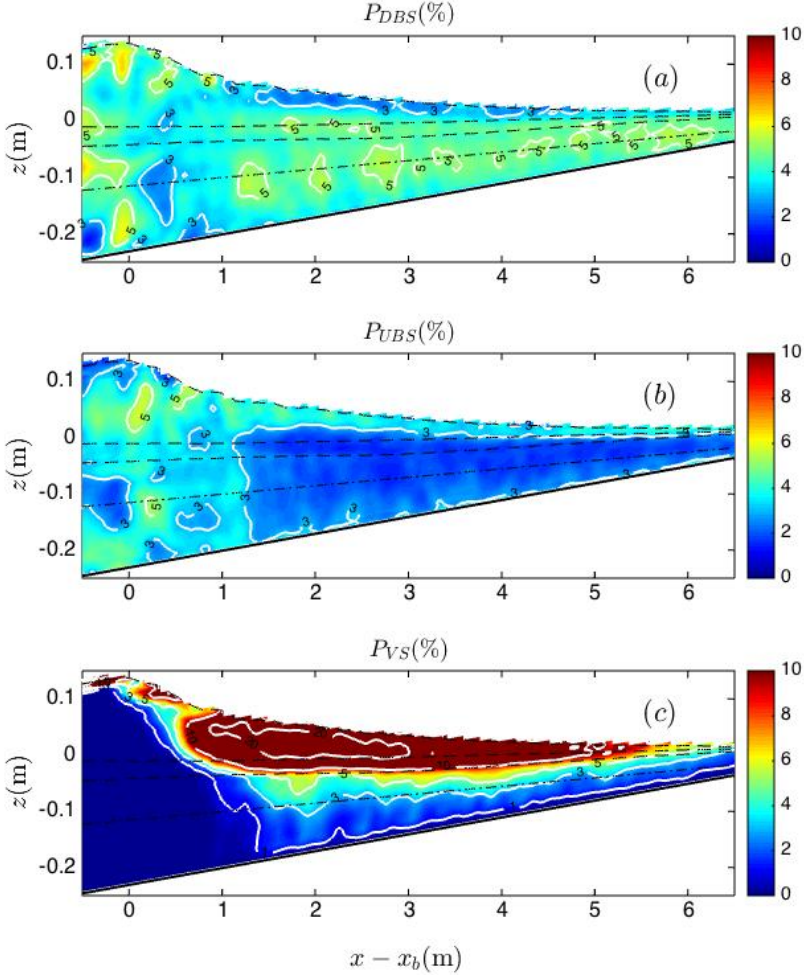


Adrian, 2007

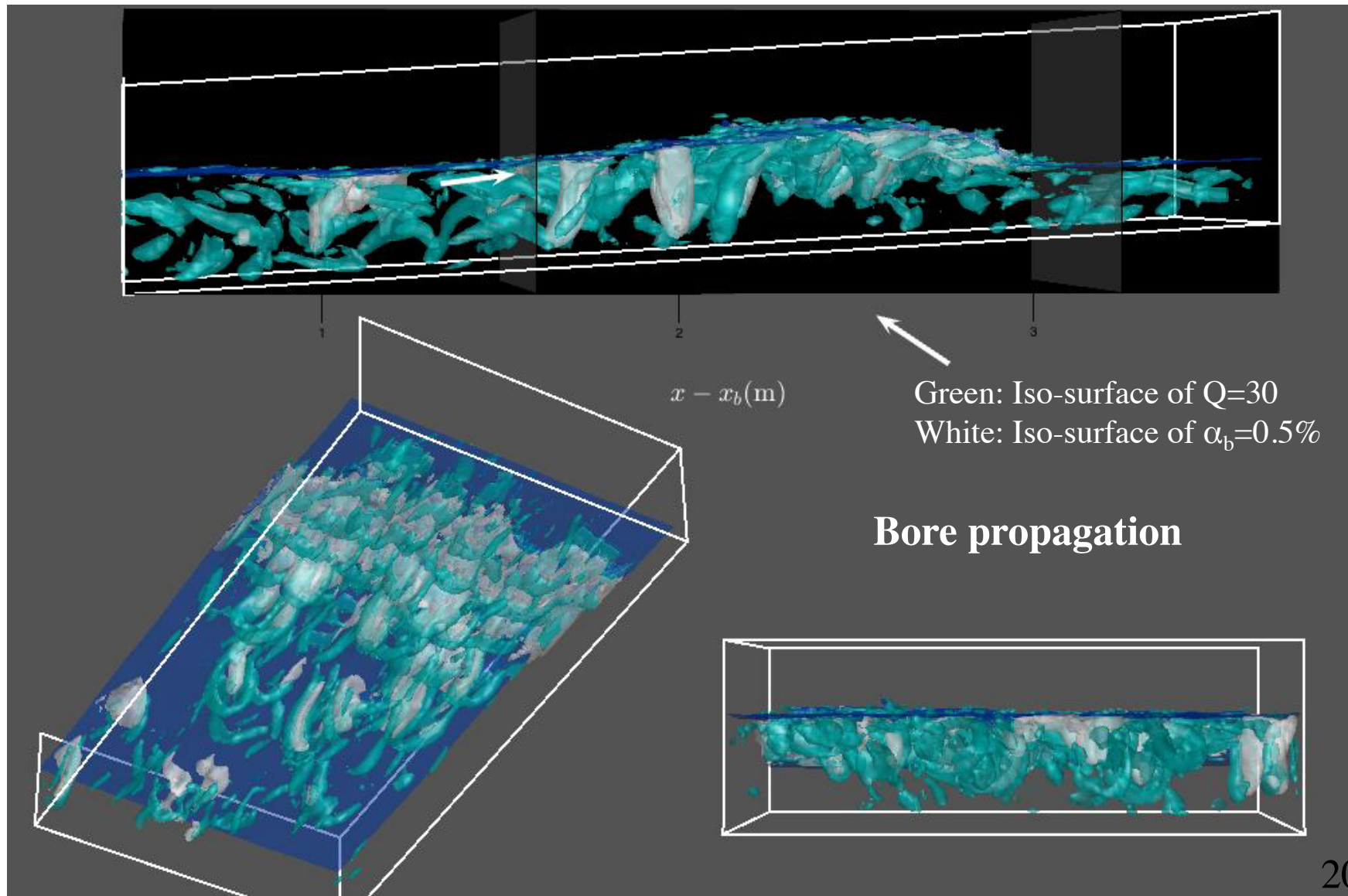
Modeled horseshoe and downburst



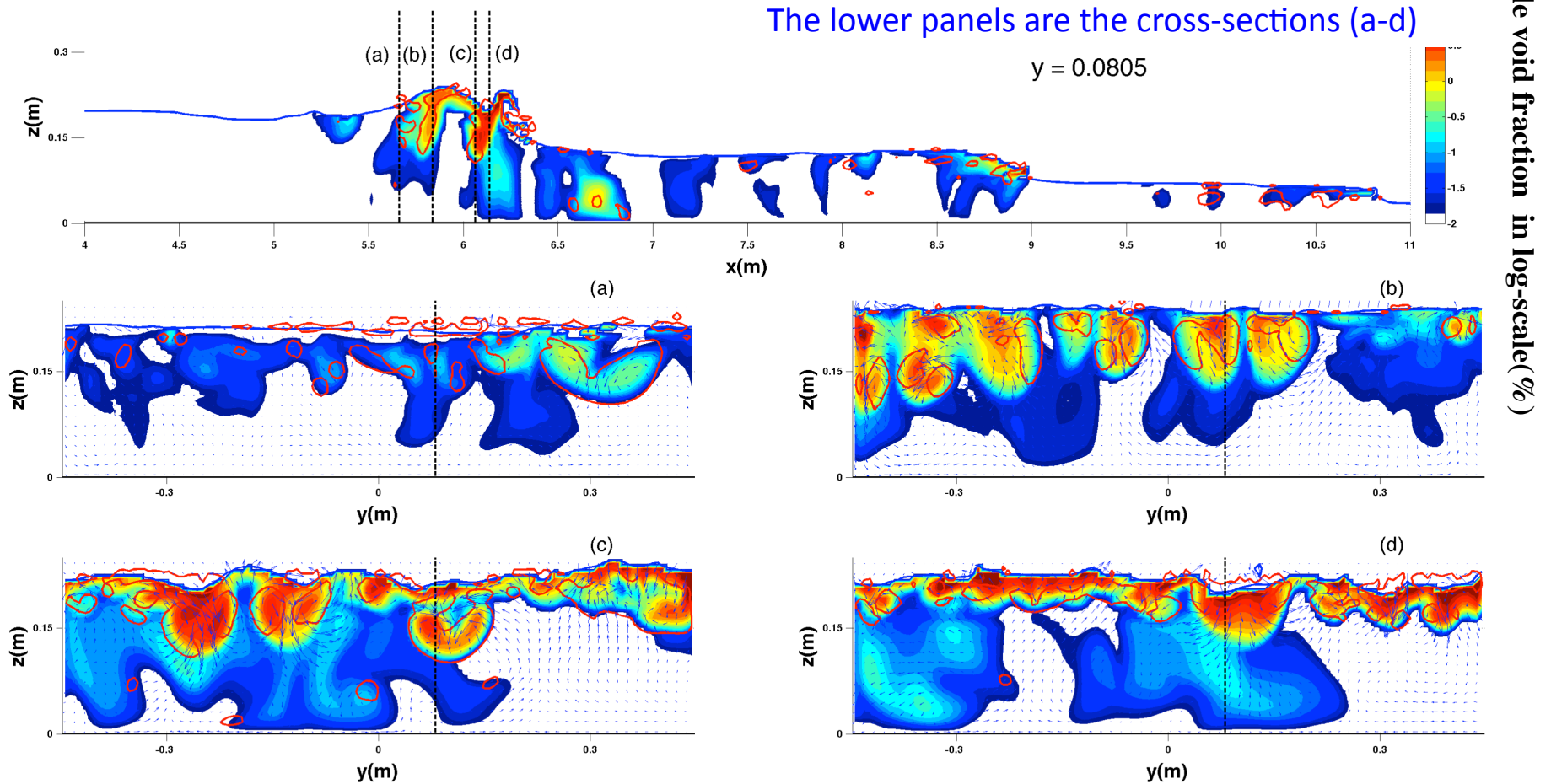
Volumes occupied by CS's, and k in each volume



What role do CS play in determining the vertical distribution of air in the water column?

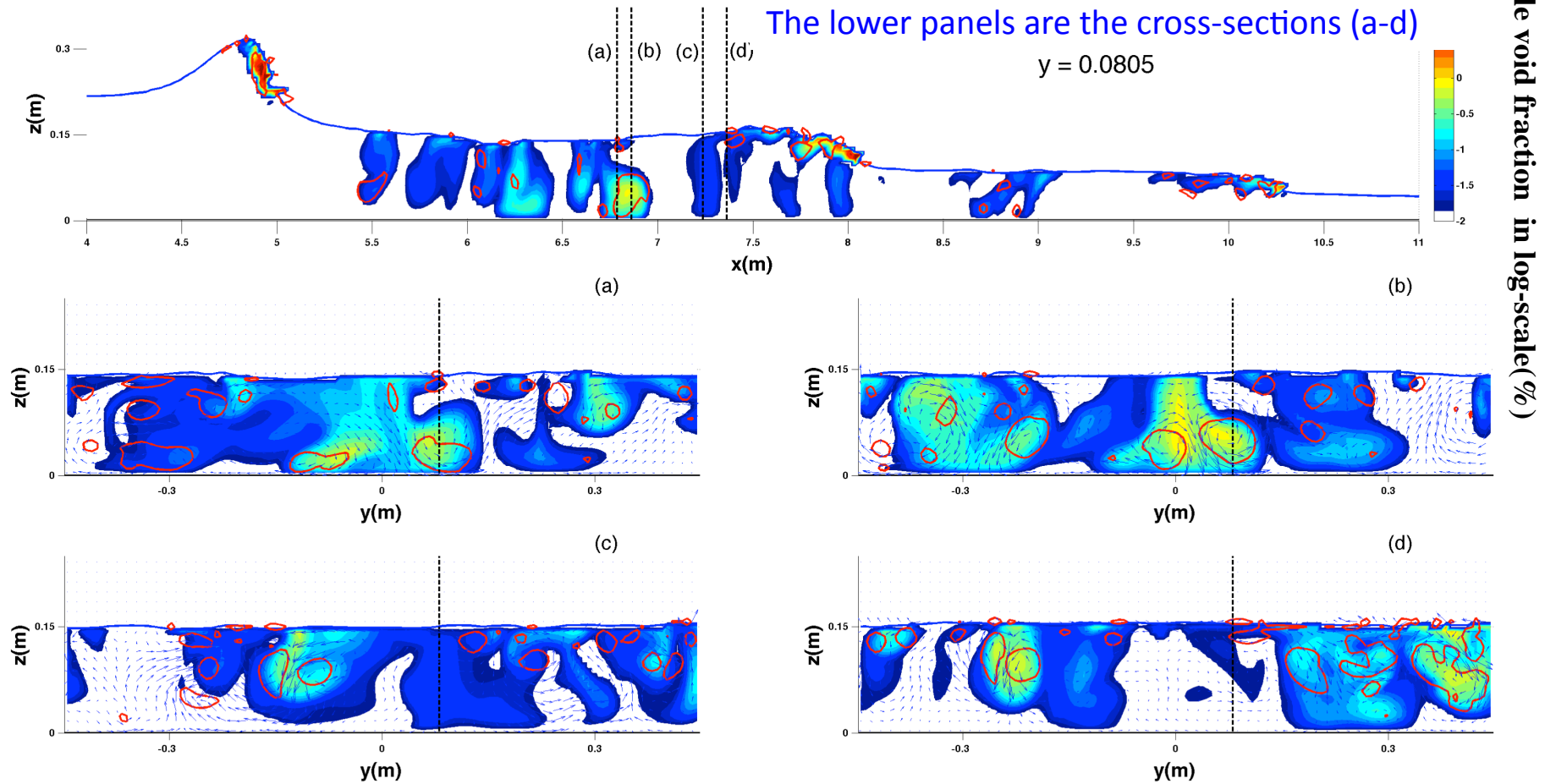


3D void fraction distribution



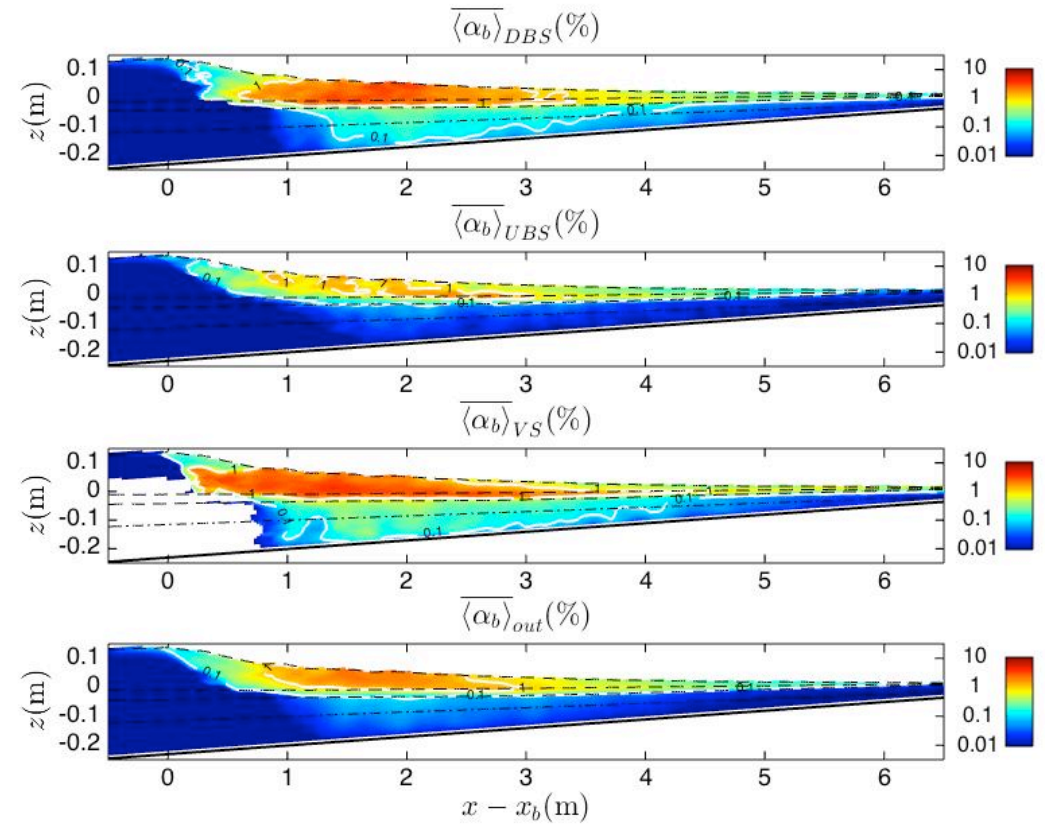
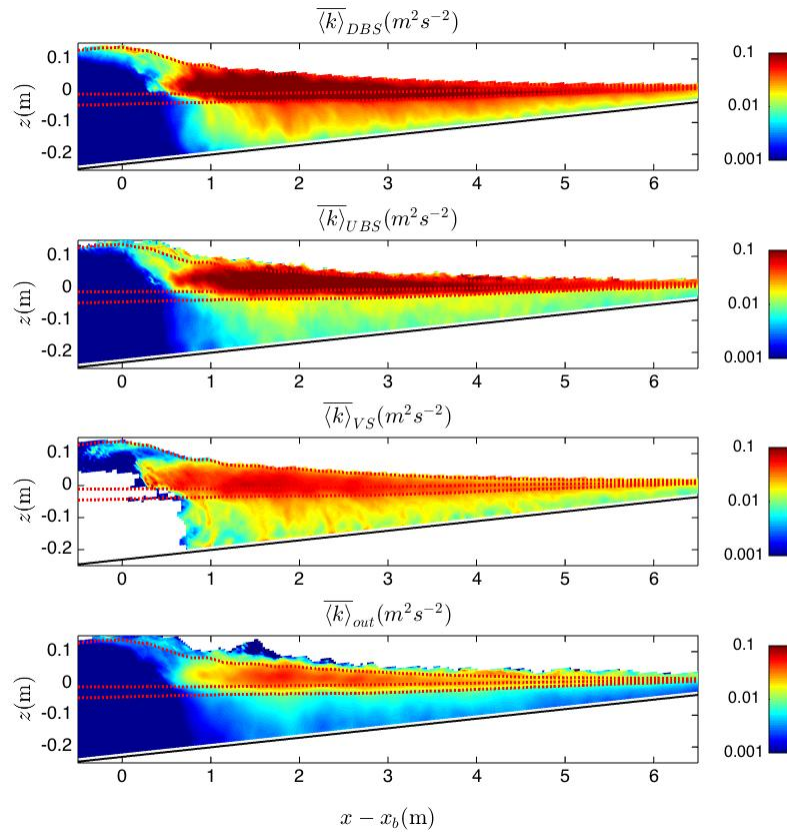
Contours are $Q = 30$
Colors show bubble void fraction in log scale

3D void fraction distribution



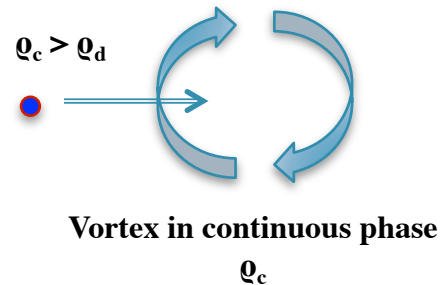
Contours are $Q = 30$
Colors show bubble void fraction in log scale

Time- and spanwise-averaged TKE and bubble void fraction inside and outside of CS



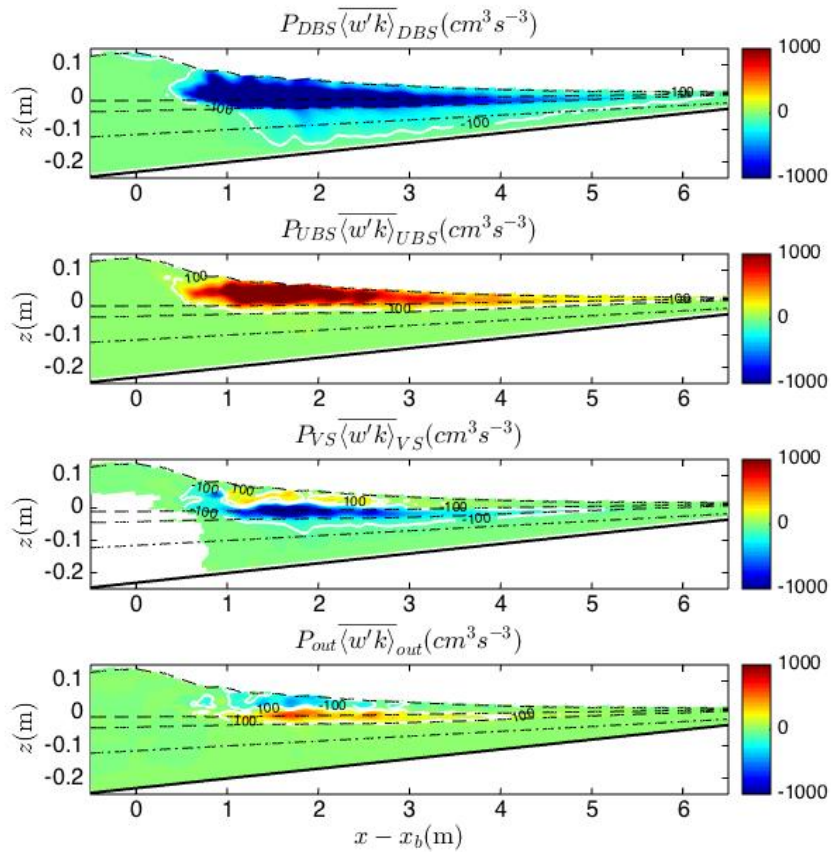
What role do the CS play in determining the vertical distribution of air in the water column?

- Bubbles may be preferentially accumulated in vortex structures (VS), and subsequently transported vertically inside the VS

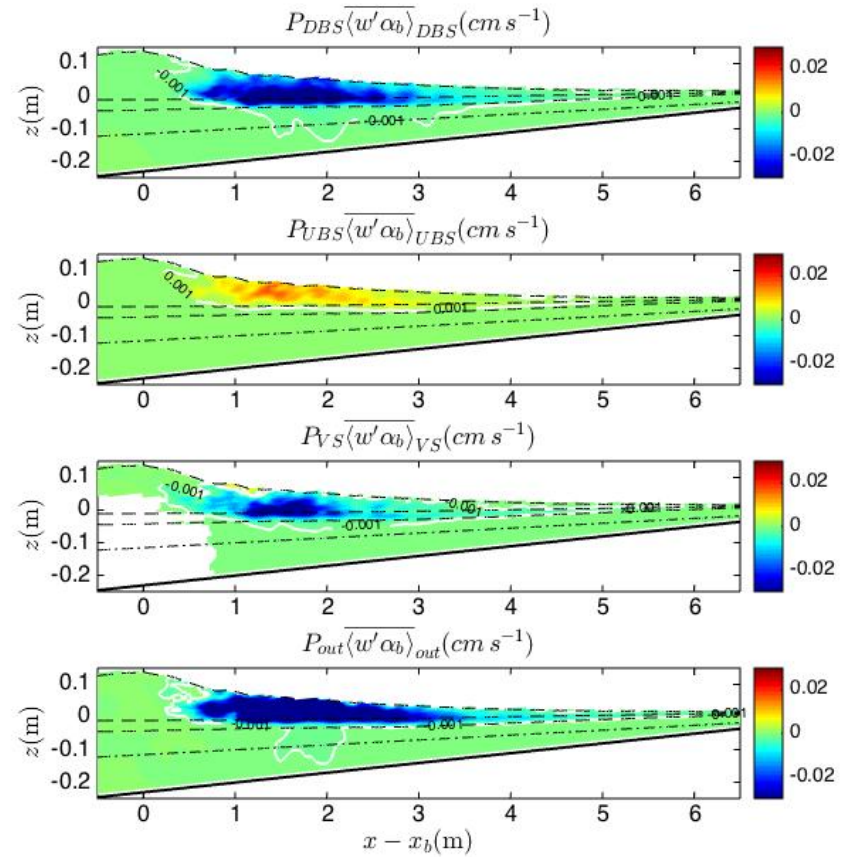


- Bubbles may also be transported by burst-like structures in a fashion similar to transport of turbulent fluctuations
- Time-averaged bubble void fractions and vertical flux rates below wave trough level inside the CS are an order of magnitude greater than outside the CS.

Vertical fluxes of turbulence and air

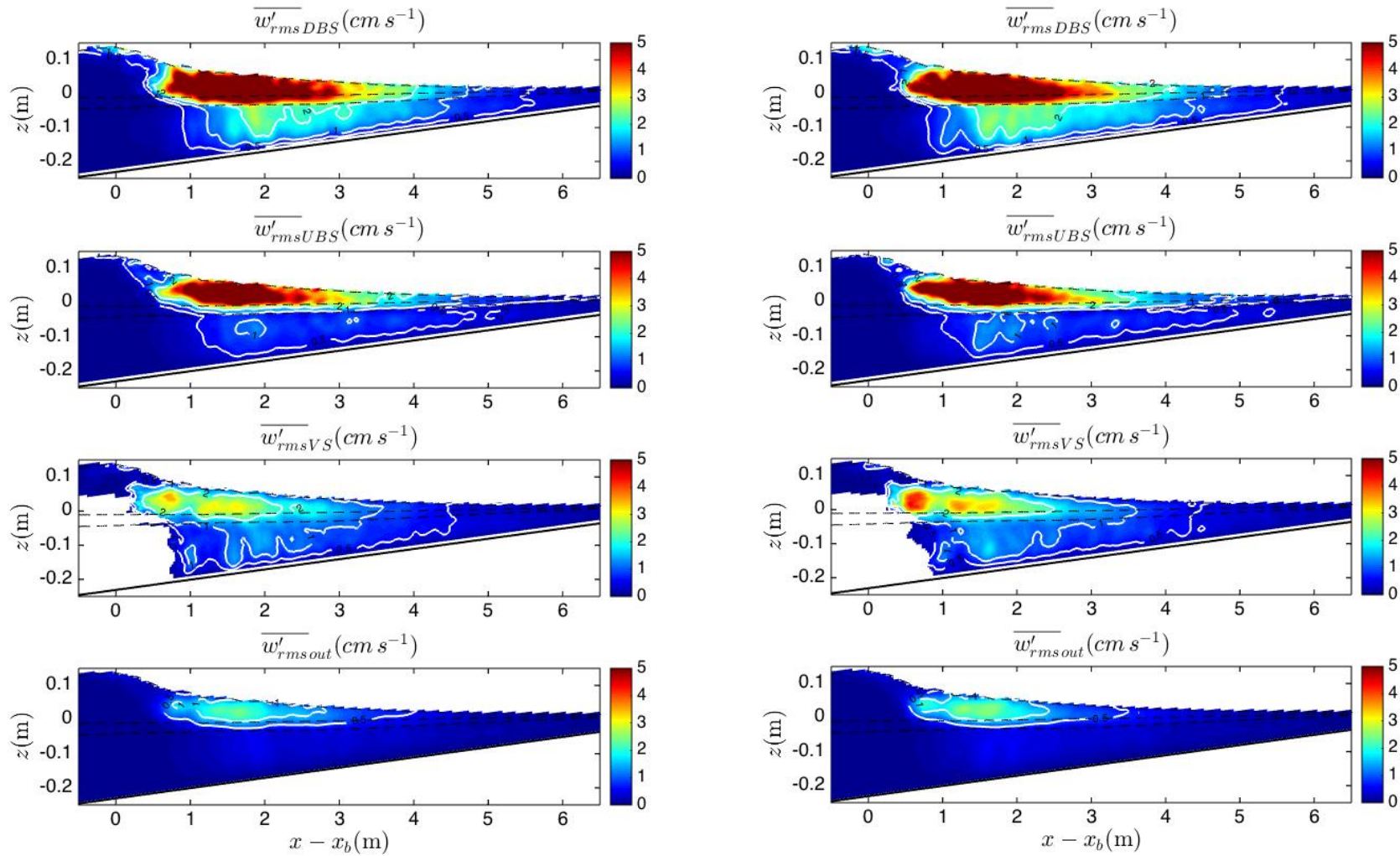


Vertical flux of k



Vertical flux of α_b

Are bubbles affecting the kinematics, dynamics?



Vertical velocity fluctuations: bubbles (left), no bubbles (right)

